ARTICLES

Journal of Semiconductors
(2021) 42, 042301
doi: 10.1088/1674-4926/42/4/042301

Monolithic DWDM source with precise channel spacing

Lianping Hou†, Song Tang, and John H. Marsh

James Watt School of Engineering, University of Glasgow, Glasgow, G12 8QQ, UK

Abstract: We report a low-cost manufacturing approach for fabricating monolithic multi-wavelength sources for dense wavelength division multiplexing (DWDM) systems that offers high yield and eliminates crystal regrowth and selective area epitaxy steps that are essential in traditional fabrication methods. The source integrates an array of distributed feedback (DFB) lasers with a passive coupler and semiconductor optical amplifier (SOA). Ridge waveguide lasers with sampled Bragg side wall gratings have been integrated using quantum well intermixing to achieve a fully functional four-channel DWDM source with 0.8 nm wavelength spacing and residual errors < 0.13 nm. The output power from the SOA is > 10 mW per channel making the source suitable for use in passive optical networks (PONs). We have also investigated using multisection phase-shifted sampled gratings to both increase the effective grating coupling coefficient and precisely control the channel lasing wavelength spacing. An 8-channel DFB laser array with 100 GHz channel spacing was demonstrated using a sampled grating with two π-phase-shifted sections in each sampling period. The entire array was fabricated by only a single step of electron beam lithography.

Key words: lasers; distributed-feedback; diode laser arrays; multiple quantum well (MQW) modulators; semiconductor optical amplifier; integrated optics devices

Citation: L P Hou, S Tang, and J H Marsh, Monolithic DWDM source with precise channel spacing[J]. *J. Semicond.*, 2021, 42(4), 042301. http://doi.org/10.1088/1674-4926/42/4/042301

1. Introduction

New approaches are needed for manufacturing optoelectronic hardware, particularly in the access network where increasing data rates need to be provided at low cost. For example, standards for the next generation of passive optical networks (PONs) envisage dense wavelength division multiplexing (DWDM) supporting aggregate data rates of 40 Gb/s[1] and beyond, and requiring optical launch powers > 10 dBm. Monolithic arrays of lasers are considered to be the most promising approach to deploy in these DWDM systems because of their high energy efficiency, small form factor, and high reliability[2]. A multi-wavelength distributed feedback (DFB) laser array requires no dynamic wavelength tuning so can be switched rapidly between WDM channels with each laser operating in a single, stable longitudinal mode (SLM)[3]. However, in such applications the wavelengths must be aligned with the International Telecommunication Union (ITU) grid in which adjacent channels are separated by 100 GHz (0.8 nm). This is done by fabricating an array where the laser wavelengths are spaced by 100 GHz and then using fine temperature and current tuning to align the whole array with the DWDM grid.

The grating period Λ of each laser is related to the Bragg wavelength through $\lambda_B = 2n_{eff}\Lambda$, where n_{eff} is the modal effective index. Assuming $n_{eff} = 3.2$, to obtain a 0.8 nm spacing for λ_B, $\Delta\Lambda$ must be as small as 0.125 nm which is beyond the classic resolution of 0.5 nm of electron beam lithography (EBL). A method for improving the resolution for grating definition beyond the standard resolution of EBL systems is therefore needed. One reported method is weighted-dose allocation variable-pitch EBL[4], but this algorithm is difficult to implement and unsuitable for volume manufacture. A second challenge is ensuring every laser operates in a SLM, which can be resolved by simplifying the whole device fabrication process. Here we use a low-cost approach to manufacturing, based on ridge waveguides with side-wall gratings and the reconstruction equivalent chirp (REC) approach, to increase the SLM yield[5, 6], the identical epitaxial layer (IEL) integration structure for electroabsorption modulators (EAMs)[7], and quantum well intermixing (QWI) to reduce the propagation loss in passive waveguides[8, 9]. Compared with the buried grating and the butt-joint and selective area growth (SAG) integration techniques, our method eliminates the need to etch and regrow the AlGaInAs active layer in different sections, avoiding Al oxidation at the etched interfaces that might otherwise impact device reliability.

We have used ridge waveguides with conventional sampled Bragg gratings (C-SBG) etched into the side-walls[10]. All lasers use the same grating period, and the operating wavelengths of individual lasers are set by the sampling period. A modified equivalent phase shift (EPS) of a quarter wavelength was placed at the center of each DFB cavity, a method which significantly increases the SLM yield[5, 6]. QWI was used to increase the bandgap of the passive waveguide sections post-growth and reduce the propagation loss. In this way, monolithically integrated DWDM sources operating at 1.55 μm with a wavelength spacing of 0.8 nm were fabricated. The chip comprises four channels (CH) of AlGaInAs/InP DFB lasers, an EAM for each laser, a passive waveguide 4 × 1 multimode-interference (MMI) coupler, and a semiconductor optical amplifier (SOA) output stage. However, the effective grating coupling coefficient κ is greatly reduced when using

Correspondence to: L P Hou, lianping.hou@glasgow.ac.uk
Received 13 OCTOBER 2020; Revised 11 NOVEMBER 2020.

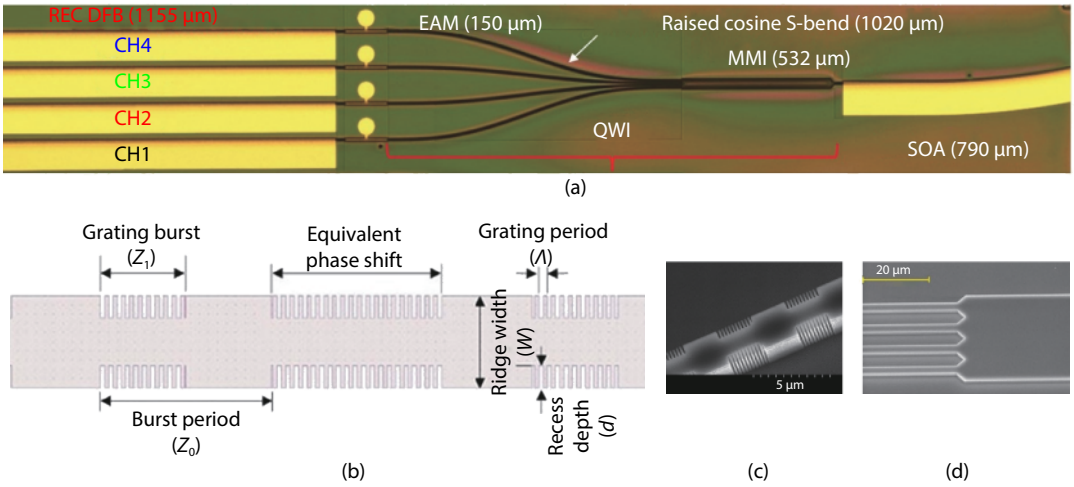

Fig. 1. (Color online) (a) DWDM source optical micrograph. (b) Illustration and relevant dimensions of the side-wall sampled grating with equivalent phase shift. (c) SEM picture of the side-wall sampled gratings. (d) Input part of the MMI coupler.

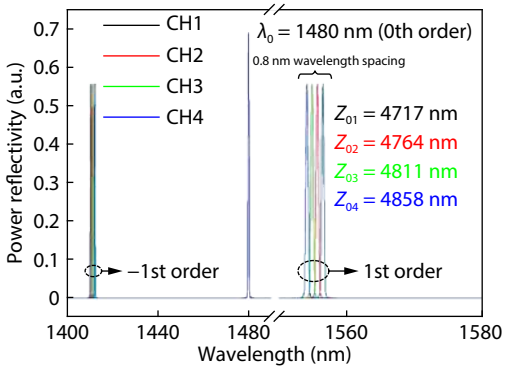

Fig. 2. (Color online) The simulated C-SBG power reflectivity of the four channels.

C-SBGs because part of the sampled period has no grating, and so we will show multi-section phase shifted sampled Bragg gratings (PS-SBGs) can be used to increase the effective κ value.

2. Device structure and fabrication

The structure of the epitaxial layers[11] and the fabrication processes[12] have been reported previously.

Fig. 1(a) shows an optical microscope picture of a single chip, together with its dimensions. The pitch between adjacent lasers was 125 μm and their ridge width was 2.5 μm. QWI was used to widen the bandgap in the MMI and S-bends by around 100 nm. The 4 × 1 MMI coupler was 30 μm-wide and 532 μm-long [Fig. 1(d)]. The raised cosine S-bends were 1020 μm-long. To minimize facet reflectivity, the SOA was fabricated as a curved waveguide terminating at an angle of 10° to the facet normal. The SOA compensated for the intrinsic loss of 6 dB of the 4 × 1 MMI coupler and allowed the output power to be increased to > 10 dBm. The SOA also can be used to shutter the output when the wavelength is being switched[13]. The four DFB lasers had the same length of 1155 μm. The common grating pitch (Λ) was 232 nm to provide a 0th order Bragg wavelength of 1.480 μm, which was deliberately designed to be far away from the gain peak at ~1.55 μm to avoid lasing in the 0th order mode (see Fig. 2). The CHl to CH4 sampled grating periods Z_0 were 4.717, 4.764, 4.811, and 4.858 μm respectively, to achieve a wavelength spacing of 0.8 nm (see Fig. 2). Z_1 was the length of the sample burst, with a 50% duty cycle ($Z_1 = Z_0/2$). The grating was of first order and was formed by etching recesses of depth d = 0.6 μm into the sidewalls of the waveguide [Fig. 1(c)] in the burst regions. The coupling coefficient of a continuous grating, κ_0, was determined using the sub-threshold spectral fitting method[14] to be ~80 cm^{-1}. The effective coupling coefficient of a sampled grating is given by $\kappa = 80/\pi = 25.5$ cm^{-1} (see Section 4 below). A $\lambda/4$ EPS was located at the center of each DFB laser [Fig. 1(b)]. The EAMs, based on the IEL scheme to simplify the fabrication process, were 150 μm-long and capable of operating data rates at > 5 Gb/s (see Fig. 4(d)).

Simulations of the power reflectivity of the sampled gratings are shown in Fig. 2, in which the waveguide internal loss of 15 cm^{-1} has been taken into account. As noted above, the operating wavelengths of the lasers were determined by the +1st order reflection peaks and lay between 1556.54 and 1554.14 nm with a spacing of 0.8 nm. The −1st order wavelengths lie around 1410 nm where the modal gain is too low to support laser operation.

3. Device performance

The DFB laser threshold currents were ~100 mA corresponding to a current density of 3.46 kA/cm^2, which is slightly higher than that of traditional buried grating ridge waveguide DFB lasers (2.29 kA/cm^2)[15].

In Fig. 3(a), it can be seen that the DFB laser wavelength can be tuned by changing its drive current, and the tuning rate was determined to be 0.013 nm/mA. When the current is held constant, the tuning coefficient is around 0.1 nm/K over the range −5 to +70 °C. The current tuning range of each DFB laser was around 2.3 nm, and the largest wavelength difference between DFB1 and DFB4 was 4.61 nm. During current tuning, no mode hopping was observed.

With I_{DFB} = 300 mA (3I_{th}), I_{SOA} = 150 mA, and V_{EAM} = 0 V, the optical spectra measured at 20 °C from the SOA side are shown in Fig. 3(b). The lasing wavelengths of the four DFB lasers were 1558, 1557.27, 1556.62, 1555.64 nm with a wavelength spacing around 0.8 nm, very close to the simula-

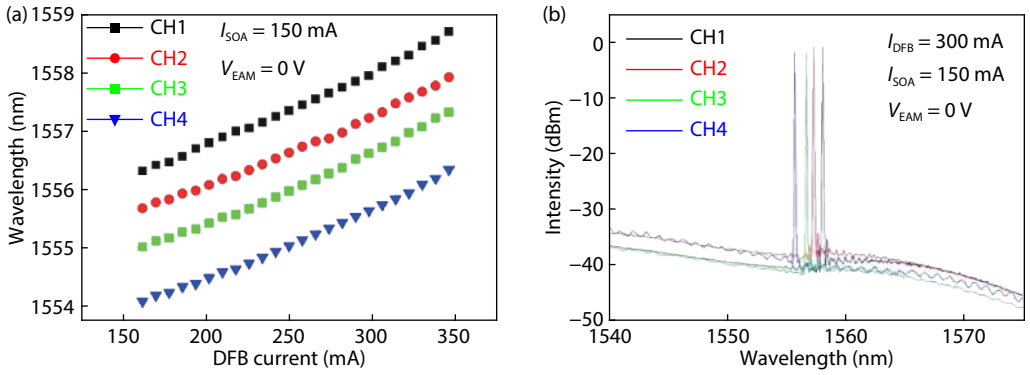

Fig. 3. (Color online) Measured from SOA side of the four channels (a) wavelengths vs I_{DFB} when I_{SOA} = 150 mA, and V_{EAM} = 0 V under 20°C, and (b) optical spectra when I_{DFB} = 300 mA, V_{EAM} = 0 V, and I_{SOA} = 150 mA under 20 °C.

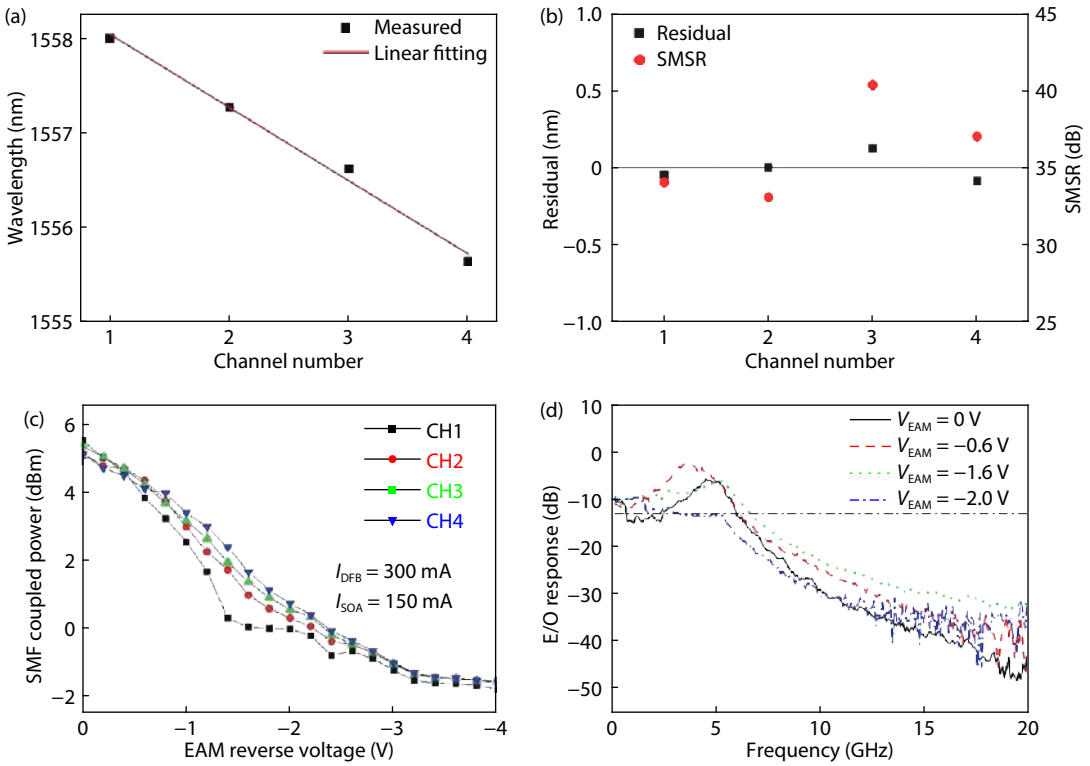

Fig. 4. (Color online) (a) Measured lasing wavelength of the four channels and the curve of its linear fitting. (b) Residual of the lasing wavelength and SMSR of the four channels. (c) Measured ER from coupled SMF of the four channels. (d) Channel 1 small signal E/O response at different V_{EAM} with I_{DFB} = 300 mA, I_{SOA} = 150 mA.

tions presented in Fig. 2 other than the measured wavelengths were redshifted due to heating at higher injection currents (300 mA).

The lasing wavelengths of the four channels from Fig. 3(b) and a linear fit with a gradient of −0.8 nm/CH are shown in Fig. 4(a). The residual error of the four channel lasing wavelengths after linear fitting of the lasing wavelengths versus the channel number is shown in Fig. 4(b). The residuals vary from −0.084 to 0.13 nm; the small magnitudes of the residuals are attributed to the precise control of the sampled grating periods, Z_0, and grating pitch, Λ, offered by EBL. The residuals can be eliminated either by slightly varying the temperature (< 1.5 °C) using a separate heater in each channel or by changing the drive current (by tuning the current by < 10 mA out of 300 mA). The measured single-mode suppression ratios (SMSRs) are shown in Fig. 4(b); all SMSRs exceed 33 dB, demonstrating excellent SLM operation of the DWDM source. By comparing the spectra from the SOA and DFB sides, it can be seen there is no degradation associated with the SOA.

The power coupled into a single mode fiber (SMF) for the four channels when I_{DFB} = 300 mA, I_{SOA} = 150 mA is shown in Fig. 4(c). The true maximum power from the SOA side should be more than 10 mW because the coupling efficiency to the SMF was less than 30%[16]. The residual output power at V_{EAM} = −4 V arises from amplified spontaneous emission in the SOA. Using an arrayed waveguide grating (AWG) combiner in place of the MMI would improve the direct current (DC) extinction ratio (ER) because the loss associated with a 4 × 1 MMI coupler is always > 6 dB. The small signal RF performance of the CH1 EAM is presented in Fig. 4(d) under the operating conditions of I_{DFB} = 300 mA, I_{SOA} = 150 mA. The −3 dB

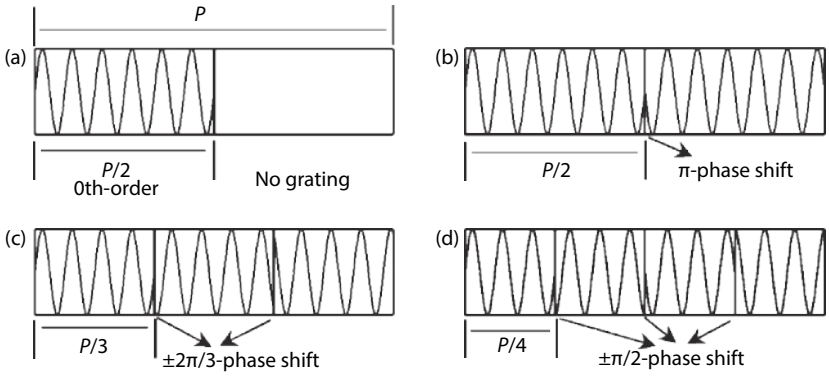

Fig. 5. Schematic structures of (a) C-SBG, (b) 2PS-SBG, (c) 3PS-SBG, and (d) 4PS-SBG. *P* is the sampling period.

bandwidth was about 6.6 GHz at $V_{EAM} = -1.6$ V, which means each channel is capable of encoding data at > 5 Gb/s. The anomalous trend of the bandwidth vs V_{EAM} in the E/O response of the EAM and the appearance of a resonance peak around the relaxation oscillation frequency indicate that there is electrical or optical coupling between the EAM and the DFB laser[7]. Electrical coupling could originate from insufficient isolation between the EAM and laser (the measured isolation resistance is about 2 kΩ) and could be reduced substantially using proton implantation[17]. Optical coupling can be attributed to residual reflections from the MMI and/or SOA. The MMI was specifically designed to reduce back-reflections, with a 45° tilt at each corner of the input and output waveguides, reducing the back reflections at the input waveguides of the MMI by at least 10 dB[18]. The major back-reflection therefore arises from the SOA output facet, which could be suppressed with an anti-reflection (AR)-coating on the output facet. Reducing the device and stray capacitance by deep etching the EAM section[19], making the bond pads smaller and using semi-insulating substrates would enable the operating speed to be increased substantially[20].

4. Multisection PS-SBG

As can be seen in Figs. 1(b) and 1(c), every sampled period of a C-SBG structure has a section where the grating is absent, which will reduce the κ value. Because the design uses ±1st-order reflections and a 50% sampling duty cycle, the effective κ is reduced to $1/\pi$ (~ 0.32) times that of the κ of a uniform grating[21]. The 0th-order reflection still has the highest reflection coefficient [Fig. 6(a)] but is displaced from the gain peak to prevent lasing at this wavelength. Recently we have proposed using multisection PS-SBGs in DFB laser arrays as these can have both high κ and precise channel spacing[22]. The grating structure of a C-SBG is shown in Fig. 5(a). Fig. 5(b) shows a design with two phase-shifted sections in a single sampling period (2PS-SBG), in which a π-phase-shifted 0th-order grating fills the half of the sampling period where there would be no grating in the equivalent C-SBG. In a 2PS-SBG structure, the 0th-order reflection disappears, and the effective κ of the ±1st-order channels is doubled compared to that of the C-SBG, with a value of $2/\pi$ (~0.64) times that of a uniform grating [Fig. 6(b)]. Similarly, the sampling period can be further divided into more sections to achieve progressively higher effective κ values. If one sampling period *P* is divided into *m* equal sections ($m > 2$), so every section has a length P/m, the phase shift between adjacent sections should be set as $\pm 2\pi/m$. The grating designs for three phase-shifted sections in a single sampling period (3PS-SBG) and four phase-shifted sections in a single sampling period (4PS-SBG) are shown in Figs. 5(c) and 5(d) respectively. The simulated reflection spectra of a 3PS-SBG and a 4-PS-SBG are shown in Figs. 6(c) and 6(d). Their effective κ values are increased to 0.83 and 0.9 times that of the uniform grating. Here the 0th-order Bragg wavelength is designed to be at 1550 nm.

The characteristics of the reflection spectra of the C-SGB, 2PS-SBG, 3PS-SBG, and 4PS-SBG and their effective κ values compared with a uniform grating are summarized in Table 1.

Using a 2PS-SBG scheme with the 0th-order sidewall grating period set at 250 nm and the sampling periods ranging from 7.979 to 9.206 μm, an eight-channel DFB laser array was fabricated with 0.837 nm channel spacing and 0.059 nm residual, as shown in Fig. 7(b)[22]. The SMSR values for all the channels are > 35 dB as shown in Fig. 7(a)[22].

Because multisection PS-SBGs have a higher κ value, it is possible to reduce the length of the DFB cavity with a corresponding reduction in the threshold current. The technique can also be used in future to fabricate directly modulated DFB lasers.

5. Conclusion

In summary, a 4-channel DWDM source suitable for use in PONs has been demonstrated by a combination of the REC, IEL, and QWI techniques. The device has an output power > 10 dBm and a channel spacing of 0.8 nm (100 GHz). The approach has the advantages of providing accurate control over the individual lasing wavelengths, offering a potentially high SLM manufacturing yield and low manufacturing costs. Using a C-SBG structure, the κ value is reduced to 0.32 times that of a uniform grating (assuming a sampling period duty cycle of 50%), but by using multisection PS-SBG designs, the κ value can be increased while maintaining precise control of the channel wavelength spacing of the DFB laser array. Based on a 2PS-SBG design, an 8-channel DFB laser array was fabricated using a single stage of EBL with a 0.837 nm channel spacing and 0.059 nm residual.

Acknowledegments

This work was supported by the U.K. Engineering and Physical Sciences Research Council (EP/R042578/1) and the National Science Foundation of China (61320106013). We would like to acknowledge the staff of the James Watt Nanofabrica-

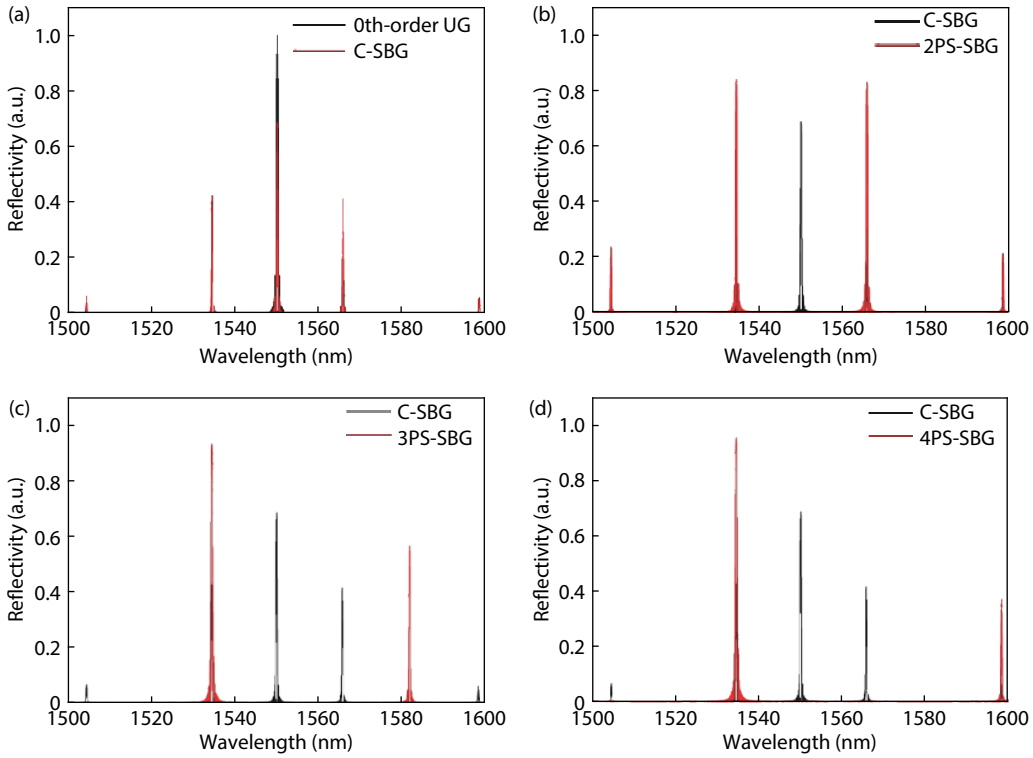

Fig. 6. (Color online) Simulated power reflection comparison between (a) uniform grating (UG) and C-SBG, (b) 2PS-SBG and C-SBG, (c) 3PS-SBG and C-SBG, (d) 4PS-SBG and C-SBG.

Table 1. Comparison between PS-SGB and C-SBG in terms of reflection characteristics and effective κ value.

No of phase step sections	Reflection spectrum characteristics	Effective κ
C-SBG	Higher 0th-order grating reflection, weaker ±1st-order reflection	0.32
2PS-SBG	0th-order reflection disappears; κ for ±1st-order doubled	0.64
3PS-SBG	0th-order reflection disappears; either +1st or −1st-order reflection disappears	0.83
4-SBG	0th-order reflection disappears; either +1st or −1st-order reflection disappears	0.90

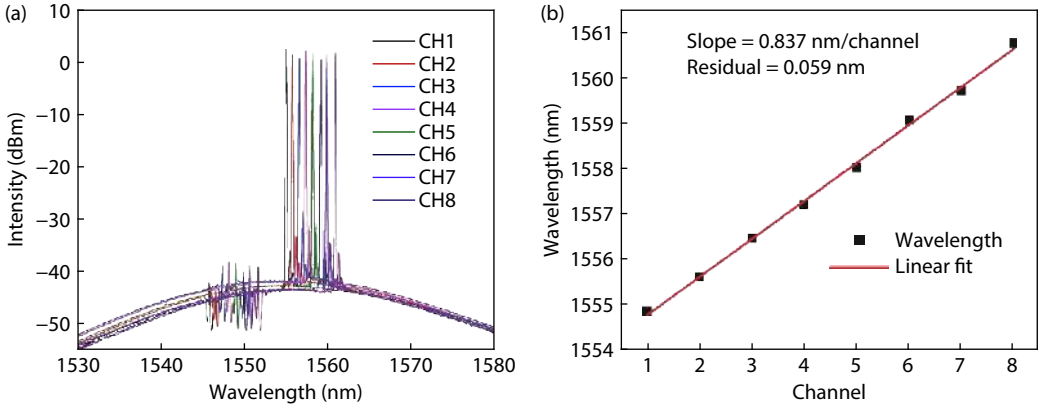

Fig. 7. (Color online) (a) Measured optical spectra of the 8-channel laser array at 100 mA (left to right, channels 1 to 8) and (b) 8-channel lasing wavelengths and the linear fitting.

tion Centre at the University of Glasgow for help in fabricating the devices.

References

[1] ITU-T RG. 989.1. 40-Gigabit-capable passive optical networks (NG-PON 2): General requirements. International Telecommunication Union, 2013

[2] Debrégeas Sillard H, Kazmierski C. Challenges and advances of photonic integrated circuits. Comptes Rendus Physique, 2008, 9, 1055

[3] Kudo K, Yashiki K, Sasaki T, et al. 1.55-μm wavelength-selectable microarray DFB-LD's with monolithically integrated MMI combiner, SOA, and EA-modulator. IEEE Photon Technol Lett, 2000, 12, 242

[4] Muroya Y, Nakamura T, Yamada H, et al. Precise wavelength control for DFB laser diodes by novel corrugation delineation method. IEEE Photon Technol Lett, 1997, 9, 288

[5] Shi Y C, Chen X F, Zhou Y T, et al. Experimental demonstration of eight-wavelength distributed feedback semiconductor laser array using equivalent phase shift. Opt Lett, 2012, 37, 3315
[6] Shi Y C, Li S M, Chen X F, et al. High channel count and high precision channel spacing multi-wavelength laser array for future PICs. Sci Rep, 2015, 4, 7377
[7] Sun C Z, Xiong B, Wang J, et al. Fabrication and packaging of 40-Gb/s AlGaInAs multiple-quantum-well electroabsorption modulated lasers based on identical epitaxial layer scheme. J Lightwave Technol, 2008, 26, 1464
[8] Hou L P, Haji M, Dylewicz R, et al. Monolithic 45-GHz mode-locked surface-etched DBR laser using quantum-well intermixing technology. IEEE Photon Technol Lett, 2010, 22, 1039
[9] Hou L P, Haji M, Dylewicz R, et al. 10-GHz mode-locked extended cavity laser integrated with surface-etched DBR fabricated by quantum-well intermixing. IEEE Photon Technol Lett, 2011, 23, 82
[10] Hou L, Haji M, Marsh J H. Mode locking at terahertz frequencies using a distributed Bragg reflector laser with a sampled grating. Opt Lett, 2013, 38, 1113
[11] Hou L P, Stolarz P, Javaloyes J, et al. Subpicosecond pulse generation at quasi-40-GHz using a passively mode-locked AlGaInAs–InP 1.55-μm strained quantum-well laser. IEEE Photon Technol Lett, 2009, 21, 1731
[12] Hou L P, Haji M, Akbar J, et al. AlGaInAs/InP monolithically integrated DFB laser array. IEEE J Quantum Electron, 2012, 48, 137
[13] Ishii H, Kasaya K, Oohashi H. Spectral linewidth reduction in widely wavelength tunable DFB laser array. IEEE J Sel Top Quantum Electron, 2009, 15, 514
[14] Nakura T, Nakano Y. LAPAREX-An automatic parameter extraction program for gain-and index-coupled distributed feedback semiconductor lasers, and its application to observation of changing coupling coefficients with currents. IEICE Trans Electron, 2000, 83(3), 488
[15] Faugeron M, Tran M, Lelarge F, et al. High-power, low RIN 1.55-μm directly modulated DFB lasers for analog signal transmission. IEEE Photon Technol Lett, 2012, 24(2), 116
[16] Hou L, Haji M, Akbar J, et al. Low divergence angle and low jitter 40 GHz AlGaInAs/InP 1.55 μm mode-locked lasers. Opt Lett, 2011, 36, 966
[17] Ramdane A, Devaux F, Souli N, et al. Monolithic integration of multiple-quantum-well lasers and modulators for high-speed transmission. IEEE J Sel Top Quantum Electron, 1996, 2, 326
[18] Hanfoug R, Augustin L, Barbarin Y, et al. Reduced reflections from multimode interference couplers. Electron Lett, 2006, 42(8), 465
[19] Weinmann R, Baums D, Cebulla U, et al. Polarization-independent and ultra-high bandwidth electroabsorption modulator in multiquantum-well deep-ridge waveguide technology. IEEE Photon Technol Lett, 1996, 8, 891
[20] Kreissl J, Bornholdt C, Gaertner T, et al. Flip-chip compatible electroabsorption modulator for up to 40 Gb/s, integrated with 1.55 μm DFB laser and spot-size expander. IEEE J Quantum Electron, 2011, 47, 1036
[21] Li J S, Cheng Y, Yin Z W, et al. A multiexposure technology for sampled Bragg gratings and its applications in dual-wavelength lasing generation and OCDMA en/decoding. IEEE Photon Technol Lett, 2009, 21, 1639
[22] Tang S, Hou L, Chen X, et al. Multiple-wavelength distributed-feedback laser arrays with high coupling coefficients and precise channel spacing. Opt Lett, 2017, 42, 1800

Lianping Hou is an Associate Professor at the University of Glasgow. His research is in semiconductor lasers, photonic integrated circuits, Terahertz transceivers. He is a senior IEEE member, an Associate Editor of Electronics Letters, Editor of American Journal of Modern Physics, and Photonics. He has authored and co-authored more than 140 journal and conference papers.

Song Tang obtained his B.S. degree from Nanjing University, Nanjing, China, in 2012, and his M.E. degree from Nanjing University, Nanjing, China, in 2015. He obtained his Ph.D. degree at the University of Glasgow, Glasgow, Scotland, in 2019. He is the author and co-author of several journal papers and conference papers and the inventor of several patents.

John H. Marsh is a Professor of Optoelectronic Systems at the University of Glasgow. His research is in integrated optics, particularly semiconductor photonic integrated circuits and semiconductor lasers. He is a Fellow of the Royal Academy of Engineering, Royal Society of Edinburgh, IEEE and OSA and a Past President (2008-9) of the IEEE Photonics Society.